Optics Letters

Octave-spanning coherent supercontinuum generation in an AlGaAs-on-insulator waveguide

Bart Kuyken,[1,2] Maximilien Billet,[1,2,3] Francois Leo,[3] Kresten Yvind,[4] and Minhao Pu[4,*]

[1]Photonics Research Group, Department of Information Technology, Ghent University IMEC, Ghent B-9000, Belgium
[2]Center for Nano- and Biophotonics (NB-Photonics), Ghent University, Ghent, Belgium
[3]OPERA-Photonique, Université Libre de Bruxelles (ULB), 50 Av. F. D. Roosevelt, CP 194/5, B-1050 Bruxelles, Belgium
[4]DTU Fotonik, Department of Photonics Engineering, Technical University of Denmark, Building 343, DK-2800 Kgs. Lyngby, Denmark
*Corresponding author: mipu@fotonik.dtu.dk

Received 28 October 2019; revised 21 November 2019; accepted 21 November 2019; posted 22 November 2019 (Doc. ID 379426); published 17 January 2020

We demonstrate supercontinuum generation over an octave spaning from 1055 to 2155 nm on the highly nonlinear aluminum gallium arsenide (AlGaAs)-on-insulator platform. This is enabled by the generation of two dispersive waves in a 3-mm-long dispersion-engineered nano-waveguide. The waveguide is pumped at telecom wavelengths (1555 nm) with 3.6 pJ femtosecond pulses. We experimentally validate the coherence of the generated supercontinuum around the pump wavelength (1450–1750 nm), and our numerical simulation shows a high degree of coherence over the full spectrum.

https://doi.org/10.1364/OL.45.000603

Supercontinuum generation (SCG), first, to the best of our knowledge, demonstrated in bulk by Alfano and Shapiro [1], is one of the most efficient ways to obtain spatially and often temporally coherent broadband light sources. It has found its way into many applications including metrology [2], telecommunication [3], spectroscopy [4], and short pulse sciences [5]. With the advent of photonic crystal fibers and their potential for tuning dispersion, the research field has undergone enormous progress in the last 20 years [6]. More recently, integrated photonic platforms have been widely used for SCG because they potentially offer a compact, low-cost solution for SCG. Various material platforms including silicon [7,8], chalcogenide [9,10], lithium niobite [11,12], and silicon nitride (Si_3N_4) [13,14] have been utilized to realize broadband SCG.

Generation of an octave-spanning supercontinuum (SC) relies on third-order ($\chi^{(3)}$) nonlinear effects. The generation of octave-spanning coherent SCG is essential for stabilizing frequency combs through f-to-2f interferometers and consequent self-referencing. This is crucial in frequency metrology and precision spectroscopy [15] applications. Apart from SCG, second harmonic generation (SHG), based on the quadratic ($\chi^{(2)}$) nonlinear process, is also required in an f-to-2f interferometer. However, because of the centrosymmetric crystal structures, materials such as silicon and Si_3N_4 lack the intrinsic $\chi^{(2)}$ effect, which inhibits the integration of the SC source and second harmonic generator in a single material platform. Although significant progress has been made to realize the effective $\chi^{(2)}$ process in silicon [16] and Si_3N_4 [17], the achieved efficiency have been limited, hampering on-chip f-to-2f interferometry. Therefore, it is highly desirable that octave-spanning SCG is realized in materials that exhibit both strong intrinsic $\chi^{(2)}$ and $\chi^{(3)}$ nonlinearities. Those materials include aluminum nitride (AlN) [18], gallium nitride [19,20], silicon carbide [21], lithium niobate [11,12,22], and (indium) gallium phosphide [23,24]. Among those materials, aluminum gallium arsenide (AlGaAs) has the strongest intrinsic Kerr coefficient (a nonlinear index of 10^{-17} m^2 W^{-1}) [25] and a strong quadratic nonlinear coefficient ($\sim$ 120 pm/v) [26]. Combining the strong material nonlinearity and high light confinement, we have developed the AlGaAs-on-insulator (AlGaAsOI) platform and demonstrated ultra-high effective Kerr nonlinearity of the platform [27]. Moreover, the bandgap of AlGaAs material can be engineered to mitigate the most detrimental nonlinear loss at the telecom wavelength induced by two-photon absorption (TPA), while the optimization of fabrication technology for this high confinement waveguide platform ensures a low linear loss, which leads to a high nonlinear figure of merit (FOM) as a Kerr nonlinear platform [28]. Recently, efficient SHG has also been demonstrated in similar high-confinement (Al)GaAsOI waveguides [29,30].

Benefiting from the ultra-high effective Kerr nonlinearity, we previously demonstrated efficient generation of a frequency comb covering the telecom C band based on self-phase modulation (SPM) by pumping an AlGaAsOI waveguide using picosecond pulses with a high repetition rate (at tens of gigahertz) for high-speed communication transmission system [31]. Very recently, Chiles *et al.* have realized suspended AlGaAs waveguides and demonstrated SCG at both the near-infrared (NIR) and mid-infrared (MIR) range by using femtosecond pulse pumping [32]. In this work, we demonstrate octave-spanning SCG in an AlGaAsOI waveguide in the NIR range through dispersive wave generation over an octave at f and 2f frequencies, which is favorable, concerning the power distribution in the generated SC for a sufficient f-to-2f self-beating

signal [33]. The coherence of the generated SC has also been verified experimentally using an interferometry method around the pump wavelength. Our numerical simulation also shows a high degree of coherence of the SC over the full octave span.

We fabricated waveguides on an AlGaAsOI wafer, where a thin AlGaAs layer on top of a low-index insulator layer resides on a semiconductor substrate. The aluminum composition of the AlGaAs layer is 21%, which corresponds to a bandgap of ~ 1.72 eV. Wafer bonding and substrate removal processes are used to fabricate the AlGaAsOI wafer [34]. Owing to the large index contrast between AlGaAs and silica, light can be confined in a sub-micron waveguide core. It not only enhances the device nonlinearity, but also enables efficient dispersion engineering, which is essential for SCG. As shown in Fig. 1, the group velocity dispersion (GVD) of the AlGaAsOI waveguide can be engineered from the normal dispersion regime (in the case of bulk AlGaAs) to the anomalous dispersion regime by tailoring its cross-sectional dimension. The waveguide exhibits a low third-order dispersion at the pump wavelength (1555 nm) and has two zero dispersion wavelengths (ZDWs) between the f and $2f$ wavelengths, which is potentially suitable for dispersive wave generation at f and $2f$ wavelengths [6].

The waveguide pattern was defined firstly in the electron-beam resist hydrogen silsesquioxane (HSQ, Dow Corning FOX-15) by electron-beam lithography (JEOL JBX-9500FS) [35]. The pattern was then transferred into the AlGaAs layer using a boron trichloride (BCl_3)-based dry etching process in an inductively coupled plasma reactive ion etching (ICP-RIE) machine. A scanning electron microscopy (SEM) picture of the etched waveguide is shown in the inset of Fig. 2, where the simulated field distribution of the fundamental TE mode is superimposed on the image. As the refractive index of HSQ is relatively low (similar to SiO_2), it was kept on top of the AlGaAs device pattern. Finally, the waveguides were clad in a 3-μm-thick silica layer using plasma enhanced chemical vapor deposition. The waveguide is inversely tapered to 120 nm at the sample facets for better input and output coupling [36].

The experimental setup is shown in Fig. 2. A femtosecond fiber laser emits 100 fs pulses with a repetition rate of 90 MHz at 1555 nm. The light is coupled to the photonic chip in free space via a focusing lens (coupling loss: 12 dB). The half-wave plate (HWP) is used to align the light to the TE polarization of the waveguide. The output of the chip is coupled to a lensed fiber (LF) (coupling loss: 4 dB). The propagation loss of the AlGaAsOI waveguide is about 2 dB/cm, which is extracted from a cut-back measurement. The output spectrum is monitored with an optical spectrum analyzer (OSA) (YOKOGAWA AQ6375B for > 1200 nm and ANDO AQ6317B for < 1200 nm). For a coherence measurement, the output spectrum is recorded after passing through a fiber-based asymmetric Mach–Zehnder interferometer containing a tunable delay (DL), a polarization controller (PC), and a variable attenuator (VOA).

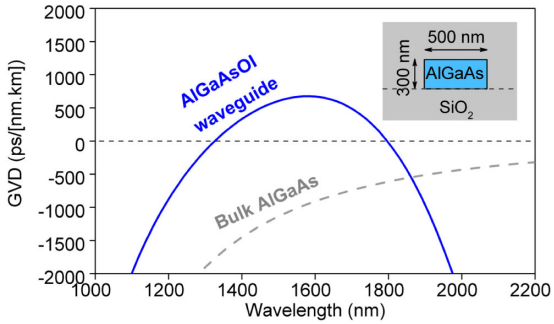

Fig. 1. Calculated group velocity dispersion (GVD) as a function of the wavelength for an AlGaAs-on-insulator (AlGaAsOI) waveguide.

The spectral broadening effects in SCG with femtosecond pulses are dominated by soliton dynamics, and the soliton number N is dependent on the peak power P by $N = \sqrt{L_D/L_{\mathrm{NL}}}$, where $L_D = (T_0^2)/|\beta_2|$ and $L_{\mathrm{NL}} = 1/\gamma P$ are the dispersion length and the nonlinear length, respectively, with T_0 the full width at half-maximum pulse duration of the injected soliton, β_2 the second-order dispersion, and γ the Kerr nonlinear coefficient of the AlGaAsOI waveguide. We characterized the output spectra with a pump peak power range that corresponds to a soliton number from 1 to 24. The measured spectrum evolution of the SCG is shown in Fig. 3(a). The black curve shows the spectrum of the coupled pump pulses with 50 fJ of energy. For clarity, throughout the paper, the pulse energies are the on-chip pulse energies. As the pump pulse energy increases, a significant broadening is observed, starting from pulse energies of 0.9 pJ. Two dispersive waves are present at around 1100 nm and 2100 nm, respectively, when the pump pulse energy reaches 3.6 pJ. The spectrum starts saturating when the pump pulse energy is increased further due to three-photon absorption (ThPA). The obtained SC has a 40 dB bandwidth of about 1100 nm covering 1055 nm to 2155 nm.

To understand the effects involved in the SCG, we model our system with a generalized nonlinear Schrödinger equation (NLSE) taking into account the Kerr nonlinearity ($630\ \mathrm{m^{-1}\ W^{-1}}$) of the AlGaAsOI waveguide [28] by using the spilt-step method [37]. The output spectra of the waveguide are then computed, as shown in Fig. 3(b). Compared with the experimental data in Fig. 3(a), the spectrum broadening effect is well reproduced by the NLSE. We can identify two distinct positions in the spectra at 1100 nm and 2100 nm, respectively, where a peak is visible. To associate a physical effect to these two peaks, we calculate the predictable frequencies of the generated dispersive waves. The phase-matching condition between the soliton centered at a frequency ω_s and a dispersive wave at a frequency ω_{DW} can be expressed by the following equation [6]:

$$\beta(\omega_{\mathrm{DW}}) = \beta(\omega_s) + (\omega_{\mathrm{DW}} - \omega_s)\, v_g^{-1} + (1 - f_R)\,\gamma P, \quad \textbf{(1)}$$

where β is the propagation constant of the wave, v_g is the group velocity at the pump frequency, f_R is the fractional Raman response, γ is the nonlinear parameter, and P is the peak power of the soliton. By neglecting the nonlinear contribution into the

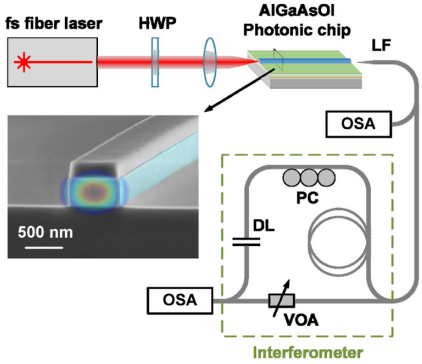

Fig. 2. Experimental setup for SCG in an AlGaAsOI waveguide. Inset shows a SEM picture of the fabricated waveguide before it has been clad in silica.

phase-matching condition, we can write the phase mismatch between a wave of frequency ω_s and the dispersive wave [14]

$$\Delta\beta(\omega) = \beta_{\text{int}} = \beta(\omega) - \beta(\omega_s) - (\omega - \omega_s)\, v_g^{-1}. \quad (2)$$

The phase matching appears when the integrated dispersion β_{int} is equal to zero. Figure 4(a) shows the calculation of β_{int} as a function of the wavelength for the AlGaAsOI waveguide. It is seen that it is possible to achieve the phase-matching condition in the NIR at 1025 nm and in the MIR at 2130 nm. Figure 4(b) presents an experimental validation of the calculated phase-matching condition by showing the recorded output spectrum of the waveguide pumped by pulses of 6.9 pJ in energy. A good agreement is observed between the calculation and the experiment for the NIR and MIR dispersive wave wavelength positions, though a small discrepancy is observed due to the fabrication imperfection, as nanometer-scale dimension perturbations may induce the shift of the dispersive waves.

The coherence of the generated SC was investigated theoretically and experimentally. The coherence $g_{12}^{(1)}$ is evaluated by using the following formula [7]:

$$g_{12}^{(1)}(\lambda) = \frac{E_1^*(\lambda)\, E_2(\lambda)}{\sqrt{|E_1(\lambda)|^2 |E_2(\lambda)|^2}}, \quad (3)$$

where E_1 and E_2 denote spectra computed from NLSE with different initial noise conditions. The input noise consists of adding one photon per mode with a random phase in the initial spectrum. In practice, we performed 20 independent simulations, and the coherence is calculated by using Eq. (3) by averaging each pair of simulated output spectra. Figure 5(a) shows the computed coherence of the generated SC obtained at different pump pulse energy. For 9.7 pJ pulse energy, it is seen

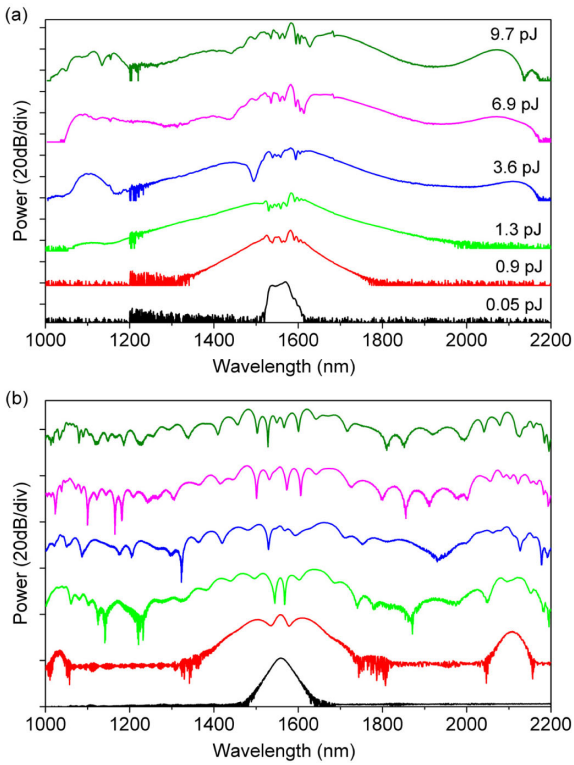

Fig. 3. Output spectra of the 500-nm-wide waveguide for different pump pulse energies. (a) Experimental data and (b) simulations.

that the parameter $g_{12}^{(1)}$ has a value close to 1 over the entire spectral range of the SC, indicating a strong coherence, which makes it promising in metrology applications that require f-to-$2f$ self-referencing.

The coherence can be estimated experimentally from the fringe visibility V of an interference pattern obtained in an interferometry measurement by using the below equation:

$$\left|g_{12}^{(1)}(\lambda)\right| = \frac{I_1(\lambda) + I_2(\lambda)}{2\sqrt{I_1(\lambda)\, I_2(\lambda)}}\, V(\lambda), \quad (4)$$

where I_1 and I_2 are the intensity from two arms of the interferometer, and $V = (I_{\max} - I_{\min})/(I_{\max} + I_{\min})$, where $I_{\max}$ and $I_{\min}$ correspond to the maxima and minima of each of the fringes. In the interferometer, as shown in Fig. 1, the VOA is used to balance the intensities of two arms, and the PC is used to align the polarization of the output light from two arms, which ensures a strong interference. Moreover, for equal intensities, the coherence can be inferred directly from the visibility [see Eq. (4)]. Figure 5(b) shows the measured output spectrum of the interferometer from 1450 nm to 1750 nm (blue curves). The bandwidth of the interferometer is limited by the fiber components, which are designed for application in the telecom band. The inset of Fig. 5(b) shows that the fringes have a relatively high contrast (about 10 dB), indicating a strong phase coherence of consequent pulses as predicted by the calculation. In Fig. 5(b), the red data points shows the extracted spectral visibility, and the majority of the data points are larger than 0.8, indicating a good coherence of the SC, limited to the resolution of the OSA.

In conclusion, we demonstrated an octave-spanning SCG in a 3-mm-long high-confinement AlGaAsOI waveguide. The coherence of the generated SC has been validated using an interferometry measurement. The waveguide dispersion was engineered to generate two dispersive waves at f and $2f$ wavelengths. Such dispersive wave generation can also enable octave-spanning Kerr comb generation in high-Q microresonators [33]. Similar to the self-referencing demonstrations in AlN [18] and Si_3N_4 [38] platforms, the AlGaAsOI platform also has the potential to realize f-to-$2f$ self-referencing by generation of a dispersive wave and a second harmonic wave at the same wavelength using a single waveguide. Thanks to the strong $\chi^{(2)}$ and $\chi^{(3)}$ nonlinearities, such a self-referencing process in the high-confinement AlGaAsOI waveguide is expected

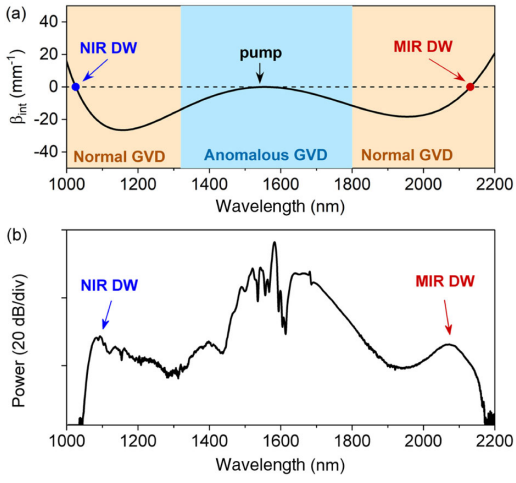

Fig. 4. (a) Calculated integrated dispersion for the AlGaAsOI waveguide. (b) The output spectrum of the AlGaAsOI waveguide with pump pulse energy of 6.9 pJ.

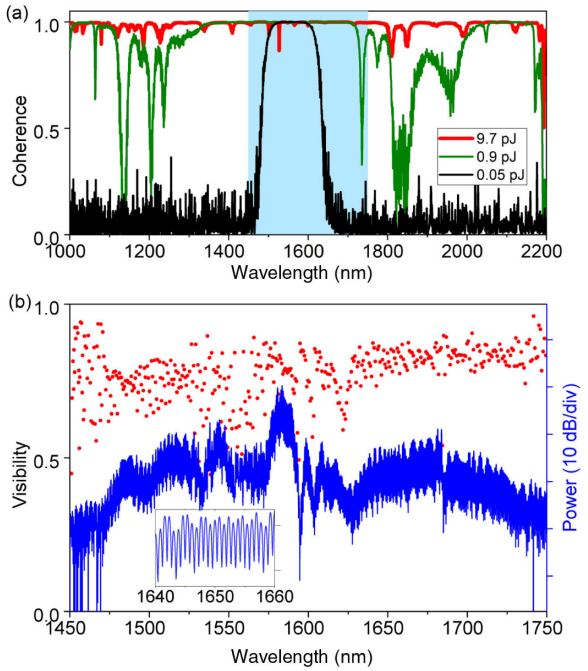

Fig. 5. (a) Simulated coherence for the SC. (b) Measured spectrum at the output of the interferometer (blue) and the extracted visibility of the spectral fringes (red). Inset shows a magnified range of the spectral fringes.

to be more efficient. Besides, the ultra-high device effective nonlinearity of the AlGaAsOI waveguide is also essential for various on-chip pulse compression techniques [39]. This makes it possible to compress picosecond pulses from on-chip mode-locked lasers [40] to femtosecond pulses, which are required for octave-spanning coherent SCG but elusive so far from on-chip lasers. Beneficial to both pulse compression and SCG, the AlGaAsOI waveguides are very promising in realization of a fully integrated octave-spanning SC source that can find applications in frequency metrology and frequency synthesis.

Funding. ELECTRIC project, European Research Council (759483); Danish National Research Council (DNRF) Center SPOC (DNRF123).

Disclosures. The authors declare no conflicts of interest.

REFERENCES

1. R. R. Alfano and S. L. Shapiro, Phys. Rev. Lett. **24**, 584 (1970).
2. D. J. Jones and S. A. Diddams, Science **288**, 635 (2000).
3. T. Morioka, K. Mori, and M. Saruwatari, Electron. Lett. **29**, 862 (1993).
4. M. J. Thorpe, Science **311**, 1595 (2006).
5. A. M. Heidt, J. Rothhardt, A. Hartung, H. Bartelt, E. G. Rohwer, J. Limpert, and A. Tünnermann, Opt. Express **19**, 13873 (2011).
6. J. M. Dudley, G. Genty, and S. Coen, Rev. Mod. Phys. **78**, 1135 (2006).
7. F. Leo, S. Gorza, S. Coen, B. Kuyken, and G. Roelkens, Opt. Lett. **40**, 123 (2015).
8. N. Singh, M. Xin, D. Vermeulen, K. Shtyrkova, N. Li, P. T. Callahan, E. S. Magden, A. Ruocco, N. Fahrenkopf, C. Baiocco, B. P.-P. Kuo, S. Radic, E. Ippen, F. X. Kärtner, and M. R. Watts, Light Sci. Appl. **7**, 17131 (2018).
9. Y. Yu, X. Gai, P. Ma, D.-Y. Choi, Z. Yang, R. Wang, S. Debbarma, S. J. Madden, and B. Luther-Davies, Laser Photon. Rev. **8**, 792 (2014).
10. J.-É. Tremblay, M. Malinowski, K. A. Richardson, S. Fathpour, and M. C. Wu, Opt. Express **26**, 21358 (2018).
11. J. Lu, J. B. Surya, X. Liu, Y. Xu, and H. X. Tang, Opt. Lett. **44**, 1492 (2019).
12. M. Yu, B. Desiatov, Y. Okawachi, A. L. Gaeta, and M. Lončar, Opt. Lett. **44**, 1222 (2019).
13. R. Halir, Y. Okawachi, J. S. Levy, M. A. Foster, M. Lipson, and A. L. Gaeta, Opt. Lett. **37**, 1685 (2012).
14. H. Guo, C. Herkommer, A. Billat, D. Grassani, C. Zhang, M. H. P. Pfeiffer, W. Weng, C.-S. Brès, and T. J. Kippenberg, Nat. Photonics **12**, 330 (2018).
15. T. Udem, R. Holzwarth, and T. W. Hänsch, Nature **416**, 233 (2002).
16. E. Timurdogan, C. V. Poulton, M. J. Byrd, and M. R. Watts, Nat. Photonics **11**, 200 (2017).
17. A. Billat, D. Grassani, M. H. P. Pfeiffer, S. Kharitonov, T. J. Kippenberg, and C.-S. Brès, Nat. Commun. **8**, 1016 (2017).
18. D. D. Hickstein, H. Jung, D. R. Carlson, A. Lind, I. Coddington, K. Srinivasan, G. G. Ycas, D. C. Cole, A. Kowligy, C. Fredrick, S. Droste, E. S. Lamb, N. R. Newbury, H. X. Tang, S. A. Diddams, and S. B. Papp, Phys. Rev. Appl. **8**, 014025 (2017).
19. C. Xiong, W. Pernice, K. K. Ryu, C. Schuck, K. Y. Fong, T. Palacios, and H. X. Tang, Opt. Express **19**, 10462 (2011).
20. E. Stassen, M. Pu, E. Semenova, E. Zavarin, W. Lundin, and K. Yvind, Opt. Lett. **44**, 1064 (2019).
21. Y. Zheng, M. Pu, A. Yi, B. Chang, T. You, K. Huang, A. N. Kamel, M. R. Henriksen, A. A. Jørgensen, X. Ou, and H. Ou, Opt. Express **27**, 13053 (2019).
22. C. Wang, C. Langrock, A. Marandi, M. Jankowski, M. Zhang, B. Desiatov, M. M. Fejer, and M. Lončar, Optica **5**, 1438 (2018).
23. U. D. Dave, C. Ciret, S.-P. Gorza, S. Combrie, A. De Rossi, F. Raineri, G. Roelkens, and B. Kuyken, Opt. Lett. **40**, 3584 (2015).
24. K. Schneider, P. Welter, Y. Baumgartner, H. Hahn, L. Czornomaz, and P. Seidler, J. Lightwave Technol. **36**, 2994 (2018).
25. J. S. S. Aitchison, D. C. C. Hutchings, J. U. U. Kang, G. I. I. Stegeman, and A. Villeneuve, IEEE J. Quantum Electron. **33**, 341 (1997).
26. I. Shoji, T. Kondo, A. Kitamoto, M. Shirane, and R. Ito, J. Opt. Soc. Am. B **14**, 2268 (1997).
27. M. Pu, L. Ottaviano, E. Semenova, and K. Yvind, Optica **3**, 823 (2016).
28. M. Pu, H. Hu, L. Ottaviano, E. Semenova, D. Vukovic, L. K. Oxenløwe, and K. Yvind, Laser Photon. Rev. **12**, 1800111 (2018).
29. L. Chang, A. Boes, X. Guo, D. T. Spencer, M. J. Kennedy, J. D. Peters, N. Volet, J. Chiles, A. Kowligy, N. Nader, D. D. Hickstein, E. J. Stanton, S. A. Diddams, S. B. Papp, and J. E. Bowers, Laser Photon. Rev. **12**, 1800149 (2018).
30. S. May, M. Kues, M. Clerici, and M. Sorel, Opt. Lett. **44**, 1339 (2019).
31. H. Hu, F. Da Ros, M. Pu, F. Ye, K. Ingerslev, E. P. da Silva, M. Nooruzzaman, Y. Amma, Y. Sasaki, T. Mizuno, Y. Miyamoto, L. Ottaviano, E. Semenova, P. Guan, D. Zibar, M. Galili, K. Yvind, T. Morioka, and L. K. Oxenløwe, Nat. Photonics **12**, 469 (2018).
32. J. Chiles, N. Nader, E. J. Stanton, D. Herman, G. Moody, J. Zhu, J. Connor Skehan, B. Guha, A. Kowligy, J. T. Gopinath, K. Srinivasan, S. A. Diddams, I. Coddington, N. R. Newbury, J. M. Shainline, S. W. Nam, and R. P. Mirin, Optica **6**, 1246 (2019).
33. D. T. Spencer, T. Drake, T. C. Briles, J. Stone, L. C. Sinclair, C. Fredrick, Q. Li, D. Westly, B. R. Ilic, A. Bluestone, N. Volet, T. Komljenovic, L. Chang, S. H. Lee, D. Y. Oh, M.-G. Suh, K. Y. Yang, M. H. P. Pfeiffer, T. J. Kippenberg, E. Norberg, L. Theogarajan, K. Vahala, N. R. Newbury, K. Srinivasan, J. E. Bowers, S. A. Diddams, and S. B. Papp, Nature **557**, 81 (2018).
34. L. Ottaviano, M. Pu, E. Semenova, and K. Yvind, Opt. Lett. **41**, 3996 (2016).
35. Y. Zheng, M. Pu, H. K. Sahoo, E. Semenova, and K. Yvind, J. Lightwave Technol. **37**, 868 (2019).
36. M. Pu, L. Liu, H. Ou, K. Yvind, and J. M. Hvam, Opt. Commun. **283**, 3678 (2010).
37. G. Agrawal, *Nonlinear Fiber Optics* (Academic, 2013).
38. D. R. Carlson, D. D. Hickstein, A. Lind, S. Droste, D. Westly, N. Nader, I. Coddington, N. R. Newbury, K. Srinivasan, S. A. Diddams, and S. B. Papp, Opt. Lett. **42**, 2314 (2017).
39. D. T. H. Tan, A. M. Agarwal, and L. C. Kimerling, Laser Photon. Rev. **9**, 294 (2015).
40. Z. Wang, K. Van Gasse, V. Moskalenko, S. Latkowski, E. Bente, B. Kuyken, and G. Roelkens, Light Sci. Appl. **6**, e16260 (2017).